Structural, spectroscopic and electronic properties of a family of bi-octahedral Ru 2 5+/6+ complexes with a bridging 2,5-di(2-pyridyl)pyrrolide ligand

Article *in* Dalton Transactions · May 2020

DOI: 10.1039/D0DT01325K

CITATIONS
0

READS
50

9 authors, including:

Bin Liu
Northwest University
139 PUBLICATIONS **2,310** CITATIONS
SEE PROFILE

John E Mcgrady
University of Oxford
235 PUBLICATIONS **5,222** CITATIONS
SEE PROFILE

Mohammed Obies
University of Babylon
2 PUBLICATIONS **0** CITATIONS
SEE PROFILE

Chao Liu
Central South University
6 PUBLICATIONS **1** CITATION
SEE PROFILE

Dalton Transactions

ROYAL SOCIETY OF CHEMISTRY

PAPER

View Article Online
View Journal | View Issue

Cite this: *Dalton Trans.*, 2020, **49**, 7053

Structural, spectroscopic and electronic properties of a family of face-shared bi-octahedral $Ru_2^{5+/6+}$ complexes with a bridging 2,5-di(2-pyridyl)pyrrolide ligand†

Shi-Rui Kang,[a] Zi-Qin Zhou,[b] Chang-Feng Xiong,[a] Bin Liu, *[b] John E. McGrady, *[c] Mohammed Obies,[c,d] Chao Liu, [a] Piao He [a] and Xiao-Yi Yi *[a]

Received 10th April 2020,
Accepted 5th May 2020

DOI: 10.1039/d0dt01325k

rsc.li/dalton

A family of Ru_2 dimers, $[Ru_2(\mu\text{-}\kappa_2N,N':\kappa_2N',N''\text{-dpp})_2(\mu\text{-}X)(X)_2]^{q+}$ (X = Cl, Br, q = 0 and X = I, q = 1) is synthesized from a $[Ru_2(OAc)_4Cl]$ paddlewheel starting material. The neutral products are mixed-valence Ru_2^{5+} dimers with a Ru–Ru bond order of 0.5, while the cationic iodide is a Ru_2^{6+} dimer with formal bond order of 1.0. The Ru–Ru distance is strikingly independent of the identity of the halide and the oxidation state of ruthenium, most likely a consequence of the small bridging nitrogen which constrains the geometry. The spectroscopic properties (EPR, UV/Vis) of the Br complex are consistent with a large σ–σ* splitting in $[Ru_2(\mu\text{-}\kappa_2N,N':\kappa_2N',N''\text{-dpp})_2(\mu\text{-Br})(Br)_2]$.

Introduction

Bimetallic units with direct covalent bonds between the metals have long held the interest of chemists and physicists, primarily due to the remarkable variations in structure, spectroscopy and magnetism.[1] More recently, it has become apparent that bimetallic units are also often uniquely suited to roles in catalysis.[2] The structural chemistry of metal dimers is diverse in the extreme, as shown in Scheme 1, from the unsupported multiply bonded species such as $[Re_2Cl_8]^{2-}$[3] through to the triply-bridged species such as $[Re_2(\mu\text{-}Cl)_3Cl_6]^-$.[4] In the unsupported cases, the dimer unit is dependent wholly on the metal–metal bond for its stability but in the bridged analogues, in contrast, metal–metal bonding is not essential, and indeed there are many examples such as $[Rh_2(\mu\text{-}Cl)_3Cl_6]^{3-}$ where it is entirely absent.[5] This has the important consequence that the cluster can adapt to changes in oxidation state without undergoing dissociation to monomeric fragments.

The paddlewheel architecture (Scheme 1a) is exemplified by the Ru_2^{5+} compound $[Ru_2(OAc)_4Cl]$ that we use as the starting material here. Since the first report of this compound by Stephenson *et al.*,[6] a large number of analogous di-ruthenium paddlewheel complexes in various oxidation states (Ru_2^{n+}, n = 4–7) have emerged in the literature.[7] These complexes are typically prepared by displacement of axial ligands such as Cl^- and/or the equatorial OAc^- ligand or, alternatively, *via* redox processes.[1,8–12] In contrast, Ru_2^{n+} complexes with the face-shared bi-octahedral geometry (Scheme 1b) are relatively less common. The electronic demands placed on bridging ligands are very different in the paddlewheel and face-shared bi-octahedral motifs: the former requires bridging ligands that present two lone pairs that lie in the same plane, while single-atom bridges are ubiquitous in the face-shared species. These differences typically manifest themselves in very different geometries, with short Ru–Ru separations in the range

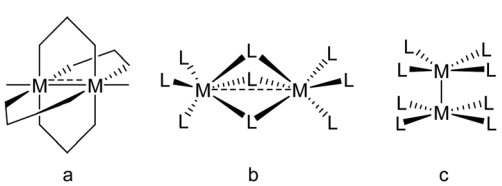

Scheme 1 The paddlewheel (a), face-shared bi-octahedral (b) and unsupported multiply bonded architecture of M_2^{n+} units (c).

[a]*College of Chemistry and Chemical Engineering, Central South University, Changsha, Hunan 410083, P. R. China. E-mail: xyyi@csu.edu.cn*
[b]*A key Laboratory of Synthetic and Natural Function Molecule Chemistry of Ministry of Education, College of Chemistry and Materials Science, Northwest University, Xi'an 710127, P. R. China. E-mail: liubin@nwu.edu.cn*
[c]*Department of Chemistry, University of Oxford, South Parks Road, Oxford OX1 3QZ, UK. E-mail: john.mcgrady@chem.ox.ac.uk*
[d]*College of Pharmacy, University of Babylon, Hilla, Iraq*

†Electronic supplementary information (ESI) available: Details of experimental methods and additional data. CCDC 1943624, 1974115, 1974117 and 1991955 for **1–3** and $Ru(dpp)_3$, respectively. For ESI and crystallographic data in CIF or other electronic format see DOI: 10.1039/d0dt01325k

2.251–2.506 Å for the paddlewheels,[1,7] and much longer distances in the face-shared bi-octahedra (2.72–3.44 Å).[13–15] Thus, direct interconversion of the two structural types represents a significant challenge.

In previous work, we have reported the ability of 2,5-di(2-pyridyl)pyrrolide (abbreviated as Hdpp) to act as a bridging-ligand between two Ru^+, Ag^+ or Cu^+ centres.[16] The dpp^- ligand binds to two metal centres *via* the two terminal pyridyl groups as well as the central nitrogen of the pyrrole ring, which acts as a bridge. The close proximity of the metal atoms in range from 2.68 to 3.13 Å results in almost negligible interactions between the centres. The coordination chemistry of the dpp^- ligand offers an interesting contrast with the closely-related di-pyridylamide ligand (dpa^-), the use of which was pioneered by both Cotton and Peng.[17,18] The dpa^- ligand also features two terminal pyridyl groups, which are linked by a single amide group rather than a pyrrole ring to form linear, fully Co–Co bonded trinuclear complexes. As a result of the monoatomic linker, the dpa^- ligands are less flexible than dpp^-, and tend to form tri-, rather than bi-metallic chains in an extension of the paddlewheel motif. In this contribution we extend the coordination chemistry of the dpp^- ligand to ruthenium by synthesizing the mixed-valence clusters $[Ru_2(\mu\text{-}\kappa_2N,N':\kappa_2N',N''\text{-}dpp)_2(\mu\text{-}X)(X)_2]$, X = Br (**1**) and Cl (**2**) along with the cationic iodide analogue, $[Ru_2(\mu\text{-}\kappa_2N,N':\kappa_2N',N''\text{-}dpp)_2(\mu\text{-}I)(I)_2]^+$ (**3**$^+$). We also present a detailed study of the spectroscopic and magnetic properties of the bromide and draw comparisons to the known chemistry of other face-shared bi-octahedra and the properties of metal–metal interaction in dinuclear metal complexes containing bridging dpp^-ligand.

Experimental

Materials, synthesis and characterization

All synthesis was carried under a nitrogen atmosphere using standard Schlenk technology unless otherwise stated. Solvents were freshly dried before use. The ^1H NMR spectra were recorded on a Bruker AVANCE(III) 400 M spectrometer. The infrared spectra (in KBr) were recorded on a Nicolet 6700 spectrometer FT-IR spectrophotometer. The UV-Vis spectra were recorded on an Agilent Technologies Cary 8454 UV-Vis at ambient temperature with a 1 cm quartz cell. The ligand Hdpp was prepared according to literature methods.[19] The diruthenium starting material $[Ru_2(OAc)_4Cl]$ was prepared as previously reported.[20] All other chemicals were obtained from J&K Scientific Ltd.

Synthesis of $[Ru_2(\mu\text{-}\kappa_2N,N':\kappa_2N',N''\text{-}dpp)_2(\mu\text{-}Br)(Br)_2]$ (1)

In a 25 mL round bottom flask equipped with a condenser and a magnetic stir bar, $[Ru_2(OAc)_4Cl]$ (0.0514 g, 0.1 mmol), Hdpp (0.0939 g, 0.4 mmol), triethylamine (58 μL, 0.42 mmol) and an excess of LiBr (0.35 g) were mixed in dried THF (5 mL). The mixture was heated to reflux overnight under nitrogen. The color of the mixture turned to brown. The solvent was removed under a vacuum. The residual solid was washed with water (10 mL × 2). The crude product was purified by column chromatography on silica gel using $CH_2Cl_2/CH_3CO_2C_2H_5$ (4 : 1, v/v) as eluent. Yield: 11 mg (26%). IR (KBr pellet, cm^{-1}): 3450(m) 3079(w) 1597(s) 1552(m) 1537(m) 1509(w) 1458(s) 1432(m) 1312(m) 1157(w) 1106(w) 1084(w) 1053(m) 950(w) 763(s) 677(w). UV-Vis: 309 nm (ε = 36 689.5 L mol^{-1} cm^{-1}), 423 nm (ε = 115 000 L mol^{-1} cm^{-1}), 479 nm (ε = 65 000 L mol^{-1} cm^{-1}), 547 nm (ε = 37 500 L mol^{-1} cm^{-1}), 665 nm (ε = 18 000 L mol^{-1} cm^{-1}). ESI-MS (*m*/*z*): 882.7695 for $[\mathbf{1} + H]^+$, calcd 882.7371. EA for $C_{28}H_{20}Br_3N_6Ru_2$ (%): cald C, 38.1; H, 2.28; N 9.52. Found C, 37.8; H, 2.39; N, 9.48.

Synthesis of $[Ru_2(\mu\text{-}\kappa_2N,N':\kappa_2N',N''\text{-}dpp)_2(\mu\text{-}Cl)(Cl)_2]$ (2)

In a 50 mL round bottom flask equipped with a condenser and a magnetic stirrer bar, $[Ru_2(OAc)_4Cl]$ (0.1 g, 0.19 mmol), Hdpp (0.19 g, 0.8 mmol), triethylamine (116 μL, 0.83 mmol) and an excess of LiCl (0.22 g) were mixed in dried THF (10 mL). The mixture was heated to reflux overnight under nitrogen, at which point the solution turned brown. The solvent was removed under a vacuum. The residual solid was washed with water (10 mL × 2). The crude product was purified by column chromatography on silica gel using $CH_2Cl_2/CH_3CO_2C_2H_5$ (4 : 1, v/v) as eluent. Yield: 5 mg (5%). IR (KBr pellet, cm^{-1}): 3457(m) 3083(w) 1598(s) 1554(m) 1535(m) 1506(w) 1456(s) 1429(m) 1316(m) 1155(w) 1108(w) 1082(w) 1056(m) 951(w) 759(s) 686(w). UV-Vis: 305 nm, 412 nm, 475 nm, 533 nm, 650 nm. ESI-MS (*m*/*z*): 750.8892 for $[\mathbf{2} + H]^+$, calcd 750.9219. EA for $C_{28}H_{20}Cl_3N_6Ru_2$ (%): cald C, 44.9; H, 2.69; N 11.2. Found C, 44.6; H, 2.78; N, 11.1.

Synthesis of $[Ru_2(\mu\text{-}\kappa_2N,N':\kappa_2N',N''\text{-}dpp)_2(I)_2(\mu\text{-}I)]\cdot I_5$ (3·I_5)

In a 25 mL round bottom flask equipped with a condenser and a magnetic stirrer bar, $[Ru_2(OAc)_4Cl]$ (0.0993 g, 0.2 mmol), Hdpp (0.184 g, 0.4 mmol), triethylamine (140 μL, 1.01 mmol) and an excess of LiI (0.22 g) were mixed in dried THF (5 mL). To exclude the water from reaction mixture, a 4 Å molecular sieve was added. The mixture was heated to reflux overnight under nitrogen, at which point the solution turned dark brown. The crude product was purified by column chromatography on silica gel using $CH_2Cl_2/CH_3CO_2C_2H_5$ (4 : 1, v/v) as eluent. Yield: 5 mg (4%). IR (KBr pellet, cm^{-1}): 3436(m) 2923(w) 1595(s) 1541(m) 1450(s) 1316(s) 1157(w) 1102(w) 760(s) 682(w). UV-Vis: 292 nm, 355 nm, 597 nm. ESI-MS (*m*/*z*): 1024.7194 for $[\mathbf{3} + H]^+$, calcd 1024.6981. EA for $C_{28}H_{20}I_7N_6Ru_2$ (%): cald C, 22.0; H, 1.32; N 5.49. Found C, 22.2; H, 1.41; N, 5.54.

ESI-MS measurements

ESI-MS was performed in a Bruker Daltonik GmbH, Bremen mass spectrometer equipped with an electrospray ionization (ESI) source. The experimental parameters were as follows: capillary temperature, 200 °C; capillary voltage, 3500 V; flow rate, 4 L min^{-1}; hexapole, 400 Vpp.

Electrochemical measurements

Cyclic voltammetry was performed on a CHI Instruments CHI610A electrochemical analyzer. This workstation contains

a digital simulation package as part of the software package to operate the workstation (CHI version 2.06). The working electrode was a glassy carbon electrode, the counter electrode is a Pt wire, and the reference electrode is a Ag/AgCl electrode in saturated KCl. Electrochemical measurements were performed in dichloromethane or acetonitrile solution containing 0.1 M tBu$_4$N·PF$_6$ electrolyte in a one compartment cell.

EPR measurement

EPR data were collected on a Bruker ELEXSYS E500 EPR spectrometer equipped with a SuperX high power microwave bridge at temperatures 80 K and 250 K, with the following parameters: X-band 9.645 GHz microwave frequency, 100 kHz modulation frequency and 2 G modulation amplitude.

Magnetic measurement

The magnetic susceptibility data were performed on a Quantum Design MPMS-XL7 SQUID magnetometer. The data were corrected for diamagnetic contributions of both the sample holder and the compound using Pascal's constants.

X-ray diffraction studies

Diffraction data was record on a Bruker CCD diffractometer with monochromatized Mo-Kα radiation (λ = 0.71073 Å). The collected frames are processed using the software SAINT. The absorption correction was processed with SADABS.[21] The structure was solved by a direct method and refined using a full matrix least squares method on F^2 with the SHELXTL software package.[22] Atomic positions of non-hydrogen atoms were refined with anisotropic parameters. All hydrogen atoms were introduced at their geometrical positions and refined as riding atoms.

Density functional theory

All calculations in this paper were performed using the ORCA suite of quantum chemical programmes.[23] Structural optimisations were performed using the BP86 functional[24] with dispersion corrections (D3-BJ).[25] TD-DFT calculations were performed in the Tamm-Dancoff approximation[26] also using the BP86 functional (450 roots) A triple-zeta polarised basis (def2-TZVP)[27] with the associated pseudopotentials was used on all non-hydrogen atoms.[28] A smaller def2-SV(P) basis sets was used on hydrogen. The RI approximation was used with the def2/J basis set.[29] The TD-DFT computed spectrum is shown in arbitrary units, scaled so that the intensity of the intense charge-transfer peaks in the experimental and simulated spectra are approximately equal.

Results and discussion

In Scheme 2, we show that treatment of [Ru$_2$(OAc)$_4$Cl], Hdpp and Et$_3$N in the presence of excess freshly dried LiBr in refluxing thf affords the face-shared bi-octahedral, mixed-valence Ru$_2^{5+}$ di-ruthenium complex [Ru$_2$(μ-κ$_2$N,N′:κ$_2$N′,N″-dpp)$_2$(μ-Br)(Br)$_2$] (**1**) in 26% yield. A similar protocol using LiCl rather

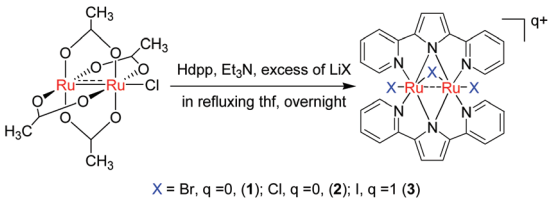

Scheme 2 The synthesis of di-ruthenium complexes with dpp$^-$ ligands.

than LiBr yields the chloride analogue, [Ru$_2$(μ-κ$_2$N,N′:κ$_2$N′,N″-dpp)$_2$(μ-Cl)(Cl)$_2$] (**2**). In contrast, using the iodide LiI results in the formation of the cationic Ru$_2^{6+}$ cluster [Ru$_2$(μ-κ$_2$N,N′:κ$_2$N′,N″-dpp)$_2$(μ-I)(I)$_2$]$^+$ (**3**$^+$) which crystallises along with a penta-iodide anion, I$_5^-$ per cation. Despite numerous efforts, we have been unable to improve on yield of these complexes. It is worth noting that the Ru^{III} mononuclear [Ru(dpp)$_3$] with about 15% yield is inevitably produced in synthesis (Fig. S1†). This provide direct visual insight into understanding the formation of Ru$_2^{5+}$ or Ru$_2^{6+}$ diruthenium complexes with low yield. Possibly, the Ru$_2^{5+}$ starting [Ru$_2$(OAc)$_4$Cl] is firstly decomposed to Ru^{II} and Ru^{III} species in refluxing thf solvent, which are captured by dpp$^-$ ligand to form **1** and **2**. Only Ru^{III} species is coordinated to dpp$^-$ligand to generate **3**$^+$ and/or [Ru(dpp)$_3$]. The dissociation and association process of dinuclear species in synthesis leads to the low yield of diruthenium products. Due to the poor yield and the huge difficulties in synthesis, the potential application of these complexes are not studied further here.

Complexes **1**, **2** and **3**$^+$ are fully characterized. The ESI mass spectrum of **1** shows a strong peak due to the protonated molecular ion ([**1** + H]$^+$) at m/z 882.7695. The ESI-MS of **2** and **3**$^+$ are also consistent with their formula. Analysis of the IR spectrum over the course of the reaction shows the disappearance of the starting material, [Ru$_2$(OAc)$_4$Cl], C=O resonance at 1400–1500 cm^{-1} and also the N–H resonance of Hdpp at 3450 cm^{-1}: both observations indicate that a dpp$^-$ ligand replaces OAc$^-$, and this is confirmed by the solid-state structure (*vide infra*). The NMR spectrum of **1** shows a number of broad peaks, consistent with its formulation as a mixed-valent species. The cyclic voltammograms of **1**, **2** and **3**$^+$ are compared in Fig. S5.† All three show a quasi-reversible redox wave (Ru$_2^{6+}$/Ru$_2^{5+}$) at ~0.30 V *vs.* Ag/AgCl and an irreversible reduction (Ru$_2^{5+}$ to Ru$_2^{4+}$) at about −0.77 V *vs.* Ag/AgCl. **3**$^+$ has a further quasi-reversible redox wave at +0.66 V due to the I$_5^-$/I$^-$ and/or I$_2$/I$^-$ couple. The relatively small separation between the oxidation and reduction waves (1.07 V) of diruthenium center is typical of systems where the unpaired electron in the mixed-valence system is delocalized over both centres.[30] The very similar cyclic voltammetry for the three complexes suggests that the isolation of the iodide as a cation rather than a neutral specie probably reflects the availability of the I$_5^-$ counter-anion rather than any fundamental difference in stability of the two oxidation states.

A solution of **1** in CH_2Cl_2 was layered in hexane to give fine darkish-brown single crystals which proved suitably for X-ray

diffraction analysis. Complex **1** is C_2 symmetric and crystallises in a triclinic lattice with space group $P2_1/c$. The structure, shown in Fig. 1, is based on a face-shared bi-octahedral architecture, with the nitrogen atoms of the two central pyrrole rings acting as bridges, along with a single bromide ligand. The coordination sphere at each ruthenium centre is then completed by two terminal pyridines from the dpp$^-$ ligand and a further bromide ligand. The dpp$^-$ ligands both have a μ-κ_2N,N′:κ_2N′,N″-coordination mode, and the coordination geometry inevitably leads to a π stacking arrangement with closest C–C contacts at ~3.30 Å. The gross structural features of **2** and **3**$^+$ are very similar to **1**, all three featuring the same μ-κ_2N,N′:κ_2N′,N″ coordination mode for dpp$^-$ along with a single bridging halide. The important bond lengths of the three clusters are compared in Table 1. The Ru1–Ru2 bond lengths in **1** and **2** are 2.5414(4) Å and 2.5450(10) Å, respectively, distinctly shorter than in typical triply-bridged Ru_2^{5+} complexes such as $[Ru_2(\mu\text{-}Cl)_3(NH_3)_6]^{2+}$ (2.753 Å),[13] $Ru_2(\mu\text{-}Cl)_3Cl_2(PBu_3)_4$ (3.28 Å) and $Ru_2(\mu\text{-}Cl)_3Cl_2(PMe_2Ph)_4$ (3.44 Å).[14,15] The distance is, in fact rather more similar to those found in quadruply-bridged species such as the $[Ru_2(OAc)_4Cl]$ starting material (2.287(2) Å), where typical values lie between 2.251 and 2.506 Å.[1,7] Unlike the di- or trinuclear complexes supported by bridging dpp$^-$ ligand, such as $[Ru_2^{I}(\mu\text{-}\kappa_2N,N':\kappa_1N''\text{-dpp})(CO)_4]$, $[Cu_2(\mu\text{-}\kappa_2N,N':\kappa_2N',N''\text{-dpp})(\mu\text{-}X)(PPh_3)_2]$, $[Ag_2(\mu\text{-}\kappa_2N,N':\kappa_2N',N''\text{-dpp})\{PO(OEt)_2\}_2]$, $[Ag(\mu\text{-}\kappa_2N,N':\kappa_2N',N''\text{-dpp})]_3$, have longer metal–metal separation (2.68 to 3.13 Å), indicating of almost negligible interactions between the centres,[16] the short Ru–Ru bonds in **1** and **2** are, at first glance, indicative of much rather stronger Ru–Ru bond than found in typical Ru_2^{5+} complexes. The bond length in the Ru_2^{6+} compound **3**$^+$ is marginally shorter, at 2.4988(15) Å. In comparing these values, it is difficult to separate the effects of changing ligand (I *vs.* Cl/Br) and oxidation state (Ru_2^{6+} *vs.* Ru_2^{5+}). However, the geometries optimized using DFT, also shown in parenthesis in Table 1, offer an opportunity to compare all three complexes over both oxidation (full details are given in ESI, Table S3†). Where comparison with experiment is possible, it is clear that the DFT calculations reproduce all of the important trends, and the optimized Ru–Ru bond lengths are within 0.03 Å of the experimental values in all cases. A like-for-like comparison then suggests that the identity of the halide has almost no influence on the Ru–Ru bond length in either oxidation state, while one-electron oxidation to the cation results in a small but systematic contraction of ~0.06 Å. This change is very much smaller than that observed in tri-halide bridged analogues. Combined with the absence of any systematic dependence on the identity of the halide, this suggests that the geometry of the Ru_2 unit is determined almost entirely by small bridging nitrogen atom which inevitably also lead to very contracted Ru–X_b–Ru angles. The bridging Ru–$N_{pyrrole}$ bond lengths are somewhat dependent on

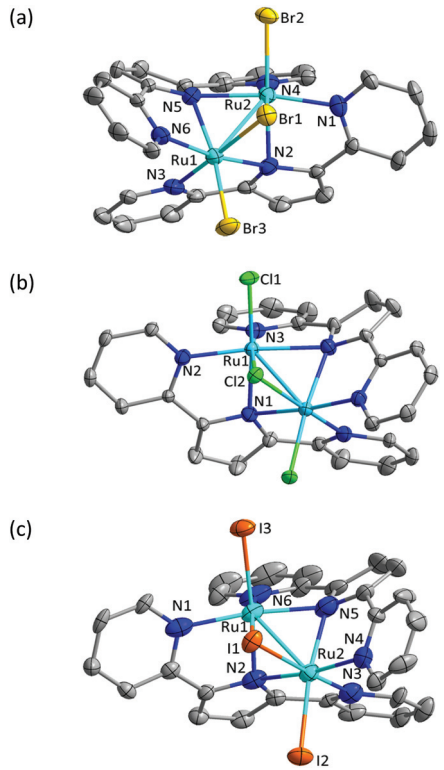

Fig. 1 The solid structures of complexes **1**(a), **2**(b) and **3**$^+$(c).

Table 1 Structural parameters of **1–3** and **1**$^+$–**3**$^+$. X-ray data are shown in bold, DFT-computed values in parenthesis

	1 (X = Br)	**1**$^+$	**2** (X = Cl)	**2**$^+$	**3** (X = I)	**3**$^+$
Ru–Ru/Å	**2.5414(4)** (2.52)	(2.46)	**2.5450(10)** (2.51)	(2.45)	(2.53)	**2.4988(15)** (2.48)
Ru–X_b/Å	**2.5352(5), 2.5392(5)** (2.58)	(2.56)	**2.4257(12)** (2.44)	(2.42)	(2.76)	**2.6974(14), 2.6961(4)** (2.74)
Ru–X_t/Å	**2.4822(6), 2.4768(5)** (2.45)	(2.43)	**2.3467(10)** (2.31)	(2.28)	(2.63)	**2.6241(14), 2.6278(14)** (2.61)
Ru–N_b (*trans* X)/Å	**2.276(3), 2.284(3)** (2.35)	(2.21)	**2.231(3)** (2.34)	(2.20)	(2.39)	**2.195(11), 2.178(12)** (2.23)
Ru–N_b (*trans* N)/Å	**2.167(3), 2.167(3)** (2.15)	(2.15)	**2.210(3)** (2.16)	(2.15)	(2.14)	**2.096(14), 2.131(13)** (2.14)
Ru–N_t/Å	**2.023(3)–2.057(3)** (2.02)	(2.04)	**2.023(3), 2.037(3)** (2.02)	(2.03)	(2.03)	**2.042(12)–2.100(14)** (2.05)
Ru–X_b–Ru/°	**60.109(13)** (58.5)	(57.4)	**63.28(4)** (62.0)	(60.7)	(54.6)	**55.20(4)** (53.8)

the trans ligand, with those *trans* to a halide ligand substantially longer than those *trans* to a pyridine group. The Ru–$N_{pyridine}$ bonds, in contrast, are short (2.023–2.057 Å) and much less dependent on the identity of the trans ligand.

The frontier Kohn–Sham orbital array in Fig. 2 shows the characteristic features of the face-shared bi-octahedral architecture,[31,32] with doubly-occupied σ and singly-occupied Ru–Ru σ* orbitals, giving a net bond order of 0.5. The configuration is therefore qualitatively similar to other face-shared bi-octahedral Ru_2^{5+} compounds such as $[Ru_2(\mu\text{-}Cl)_3Cl_6]^{4-}$.[33] One-electron oxidation removes the electron in the σ* orbital, generating a closed-shell singlet state with a formal Ru–Ru bond order of 1.0 and the somewhat shorter bond lengths reported in Table 1.

The ground-state electronic structure offers a platform for interpreting the magnetic susceptibility of **1**, and also its EPR and UV/Visible spectroscopy. Powder EPR spectra collected at both 80 K and 250 K are identical (Fig. 3A), and show a axial signal with g values of $g_x = g_y = 2.078$ and $g_z = 1.992$. For comparison, Fig. 3 Magnetic properties of **1**: (A) powder EPR spectra at 80 K and 250 K and (B) χ_M and $\chi_M T$ *versus* T DFT-computed g values based on the ground-state electronic structure described in Fig. 2 are $g_x = 2.051$, $g_y = 2.052$ and $g_z = 2.012$: the slight splitting of the g_x and g_y components reflects the inequivalence of the x and y axes in C_2 symmetry, but the splitting is clearly not large enough to be resolved in the experiment. An axial spectrum is typical of face-shared bi-octahedral Ru_2^{5+} systems, but the anisotropy is less pronounced than it is in $[Ru_2(\mu\text{-}Cl)_3(NH_3)_6]^{2+}$, for example, where $g_x = g_y = 2.100$ and $g_z = 1.950$.[31,34] The anisotropy of the g tensor can be traced to large off-diagonal elements of the spin–orbit operator between the δ/π and σ* orbitals shown in Fig. 2, and the relatively low values of g_x and g_y in **1** are therefore consistent with a high-lying σ* orbital and hence strong Ru–Ru bonding.

The plots of $\chi_M T$ and χ_M *versus* T for **1** in the temperature range of 1.8–300 K are shown in Fig. 3B. The room temperature $\chi_M T$ value is 0.417 cm^3 K mol^{-1} ($\mu_{eff} = 1.826\mu_B$), somewhat higher than the spin-only value for an $S = 1/2$ paramagnet ($\mu_{eff} = 1.732\mu_B$). Upon cooling, $\chi_M T$ decrease slowly down to 20 K before dropping to a 0.219 cm^3 K mol^{-1} ($\mu_{eff} = 1.323\mu_B$) at 1.8 K. Fitting the molar magnetic susceptibility to the Curie–Weiss law $\chi_M = C/(T - \theta)$, yields a Curie constant $C = 0.418$ cm^3 mol^{-1} K and $\theta = -2.84$ K: the negative θ value suggests the presence of weak antiferromagnetic interactions between neighbouring Ru_2^{5+} dimers in the crystalline lattice.

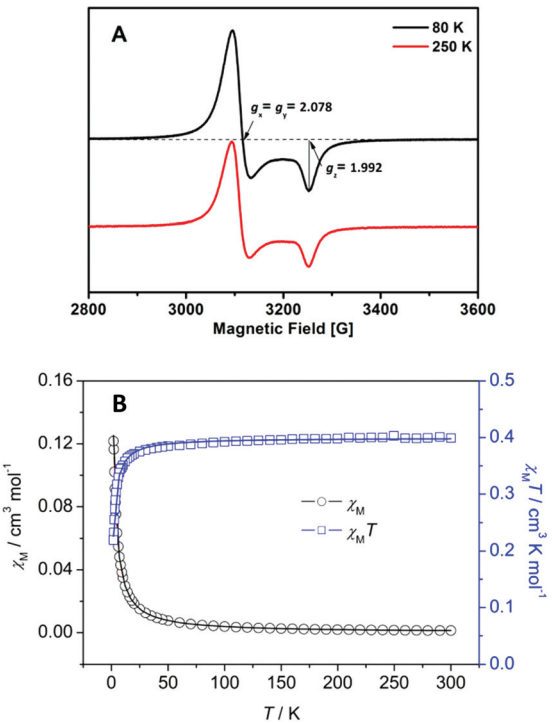

Fig. 3 Magnetic properties of **1**: (A) Powder EPR spectra at 80 K and 250 K and (B) χ_M and $\chi_M T$ *versus* T.

The UV/Vis absorption spectrum of **1** shown in Fig. 4 is strikingly different from that of the $Ru_2(OAc)_4Cl$ starting material (Fig. S4†), with absorption bands in region of 220–350 nm and 428 nm. The simulated spectrum calculated

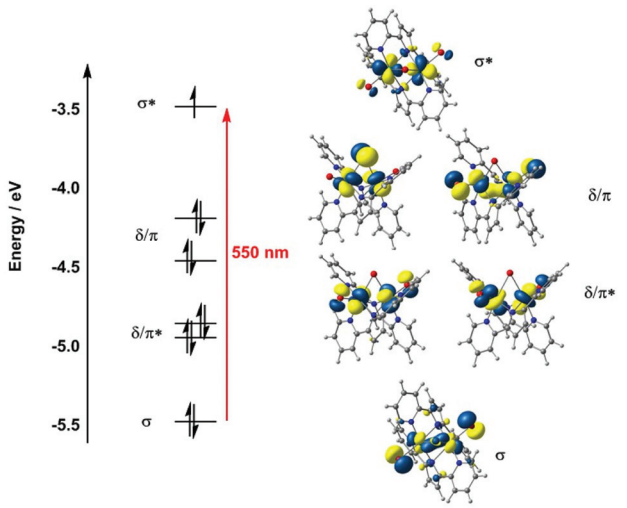

Fig. 2 Frontier Kohn–Sham orbitals of **1**. Only the spin-β manifold is shown. The red arrow marks the σ → σ* transition.

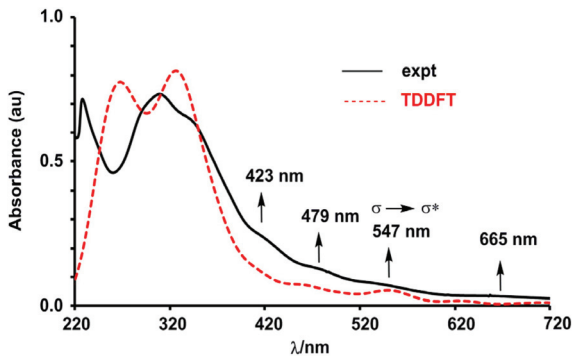

Fig. 4 UV-vis spectrum of complex **1** (concentration of **1** is 2 μM) in CH_2Cl_2 and its TD-DFT computed spectrum.

with time-dependent density functional theory (TD-DFT, BP86 functional), also shown in Fig. 4 (red dashed line), reproduces the key features of the experimental data. The intense features below 400 nm have contributions from a large number of individual transitions, dominated by both intra-ligand π–π* transitions and Br → Ru charge transfer. In the closely-related tri-halide bridged "ruthenium blues" such as $[Ru_2(\mu\text{-}Cl)_3(NH_3)_6]^{2+}$ and $[Ru_2(\mu\text{-}Cl)_3Cl_6]^{4-}$, the strongly dipole-allowed σ → σ* transition is usually a prominent feature in the visible or near-IR region of the spectrum (typically above 800 nm).[31,33,34] The TD-DFT calculations on **1** show two moderately intense transitions around 550 nm, both with significant contributions from the σ → σ* one-electron excitation. There is no distinct feature in the spectrum in this region, but there is a shoulder at 547 nm on the rising edge of the charge transfer manifold that we tentatively assign to this transition. The substantial shift to shorter wavelengths compared to the tri-halide bridged blues is a result of the very short Ru–Ru bond, which imposes a greater splitting of the σ/σ* manifold.

Conclusions

In summary, we have reported here the synthesis, structure, electrochemistry and magnetism of a new family of face-shared bi-octahedral di-ruthenium complexes $[Ru_2(\mu\text{-}\kappa_2N,N':\kappa_2N',N''\text{-}dpp)_2(\mu\text{-}X)(X)_2]^{q+}$ from paddlewheel precursor $[Ru_2(OAc)_4Cl]$, maybe involving in a dissociation and association process of dinuclear species in synthesis. Usually, the Ru–Ru separations in known face-shared bi-octahedra geometry has relative long (3.28–3.44 Å) resulting in almost negligible interactions between the centres. Herein, we found that nitrogen donor dpp^- ligand is flexible and provides a platform for aggregation of Ru^{2+} and/or Ru^{3+} to give face-shared bi-octahedra mixed-valence Ru_2^{5+} dimers with a Ru–Ru bond order of 0.5, and a Ru_2^{6+} dimer with formal bond order of 1.0. In some sense, this is a new type of face-shared bi-octahedra structure featuring of distinct metal–metal bond between two ruthenium centres. The theoretic analysis displays that the relative insensitivity of the bond lengths to either halide or oxidation state reflects the constraining effect of the small pyrrole nitrogen bridges from dpp^- ligand. The spectroscopic and magnetic properties of **1** are all consistent with a delocalized (Robin-Day class III) mixed-valence Ru_2^{5+} dimer, with a single unpaired electron delocalized over both metal centres in the σ* orbital.

Conflicts of interest

There are no confilicts to declare.

Acknowledgements

This work was supported by the National Natural Science Foundation of China (project 21571190 and 21673172) and The Natural Science Foundation of Shanxi Province (no. 2020JM-435). M. O acknowledges the HCED in Iraq for a scholarship.

Notes and references

1 (*a*) F. A. Cotton, C. A. Murillo and R. A. Walton, *Mutiple Bonds Between Metal Atoms*, Spinger Science and Business Media, Inc, New York, 2005, pp. 377–430; (*b*) S. T. Liddle, *Molecular Metal-Metal Bonds: Compounds, Synthesis, Properties*, Wiley-VCH, Weinheim, Germany, 2015, pp. 225–278.
2 I. G. Powers and C. Uyeda, *ACS Catal.*, 2017, **7**, 936–958.
3 F. A. Cotton and C. B. Harris, *Inorg. Chem.*, 1965, **4**, 330–333.
4 G. A. Heath, J. E. McGrady, R. G. Raptis and A. C. Willis, *Inorg. Chem.*, 1996, **35**, 6838–6843.
5 F. A. Cotton and D. A. Ucko, *Inorg. Chim. Acta*, 1972, **6**, 161–172.
6 T. A. Stephenson and G. Wilkinson, *J. Inorg. Nucl. Chem.*, 1966, **28**, 2285–2291.
7 M. Cortijo, R. González-Prieto, S. Herrero, J. L. Priego and R. Jiménez-Aparicio, *Coord. Chem. Rev.*, 2019, **400**, 213040–213062.
8 G. M. Chiarella, F. A. Cotton, C. A. Murillo, K. Ventura, D. Villagran and X. P. Wang, *J. Am. Chem. Soc.*, 2014, **136**, 9580–9589.
9 S. Ngubane, K. M. Kadish, J. L. Bear, E. V. Caemelbecke, A. Thuriere and K. P. Ramirez, *Dalton Trans.*, 2013, **42**, 3571–3580.
10 G. L. Xu, A. Cordova and T. Ren, *J. Cluster Sci.*, 2004, **15**, 413–424.
11 J. S. Pap, J. L. Snyder, P. M. Piccoli and J. F. Berry, *Inorg. Chem.*, 2009, **48**, 9846–9852.
12 P. Angaridis, F. A. Cotton, C. A. Murillo, D. Villagran and X. P. Wang, *J. Am. Chem. Soc.*, 2005, **127**, 5008–5009.
13 M. N. Hughes, D. O'Reardon, R. K. Poole, M. B. Hursthouse and M. Thornton-Pett, *Polyhedron*, 1987, **6**, 1711–1713.
14 F. A. Cotton and R. C. Torralba, *Inorg. Chem.*, 1991, **30**, 2196–2207.
15 (*a*) J. Bravo, J. Castro, S. García-Fontán, M. C. RodrÍguez-MartÍnez and P. RodrÍguez-Seoane, *Eur. J. Inorg. Chem.*, 2006, 3028–3040; (*b*) G. Cavigliasso, T. Lovell and R. Stranger, *Dalton Trans.*, 2006, 2017–2025.
16 (*a*) X. H. Hu, Y. Liang, C. Li and X. Y. Yi, *Dalton Trans.*, 2014, **43**, 2458–2464; (*b*) Y. P. Wang, J. J. Xiao, X. H. Hu and X. Y. Yi, *Inorg. Chim. Acta*, 2015, **435**, 125–130; (*c*) T. T. Zhang, H. Q. Xiao, S. Q. Liu, W. H. Leung, Y. Wang, W. H. Zhu, X. Liang and X. Y. Yi, *J. Organomet. Chem.*, 2019, **896**, 102–107.
17 E. C. Yang, M. C. Cheng, M. S. Tsai and S. M. Peng, *J. Chem. Soc., Chem. Commun.*, 1994, 2377–2378.
18 F. A. Cotton, L. M. Daniels and G. T. Jordan IV, *Chem. Commun.*, 1997, **5**, 421–422.

19 R. A. Jones, M. Karatza, T. N. Voro, P. U. Civeir, A. Franck, O. Ozturk, J. P. Seaman, A. P. Whitmore and D. J. Williamson, *Tetrahedron*, 1996, **52**, 8707–8724.
20 T. A. Stephenso and G. Wilkinson, *J. Inorg. Nucl. Chem.*, 1966, **28**, 2285–2291.
21 G. M. Sheldrick, *SADABS, Empirical Absorption Correction Program*, University of Göttingen, Germany, 1997.
22 G. M. Sheldrick, *SHELXTL-Plus V5.1 Software Reference Manual*, Bruker AXS Inc., Madison, Wisconsin, USA, 1997.
23 ORCA 4.0, *WIREs Comput. Mol. Sci.*, 2018, **8**, e1327.
24 (*a*) A. D. Becke, *J. Chem. Phys.*, 1993, **98**, 1372–1375; (*b*) J. P. Perdew and Y. Wang, *Phys. Rev. B: Condens. Matter Mater. Phys.*, 1992, **45**, 13245.
25 (*a*) E. R. Johnson and A. D. Becke, *J. Chem. Phys.*, 2006, **124**, 174104; (*b*) S. Grimme, S. Ehrlich and L. J. Goerigk, *Comput. Chem.*, 2011, **32**, 1456–1465.
26 S. M. Dancoff, *Phys. Rev.*, 1950, **78**, 382–385.
27 F. Weigend and R. Ahlrichs, *Phys. Chem. Chem. Phys.*, 2005, **7**, 3297–3305.
28 D. Andrae, U. Haeussermann, M. Dolg, H. Stoll and H. Preuss, *Theor. Chim. Acta*, 1990, **77**, 123–141.
29 F. Weigend, *Phys. Chem. Chem. Phys.*, 2006, **8**, 1057–1065.
30 J. Darriet, *Rev. Chim. Miner.*, 1981, **18**, 27.
31 B. D. Yeomans;, D. G. Humphrey and G. A. Heath, *J. Chem. Soc., Dalton Trans.*, 1997, **22**, 4153–4166.
32 G. A. Heath and J. E. McGrady, *J. Chem. Soc., Dalton Trans.*, 1994, 3759–3767.
33 B. J. Kennedy, G. A. Heath and T. J. Khoo, *Inorg. Chim. Acta*, 1991, **190**, 265–269.
34 L. Dubicki and E. Krausz, *Inorg. Chem.*, 1985, **24**, 4461–4465.